Materials Chemistry and Physics 111 (2008) 82–86

Contents lists available at ScienceDirect

Materials Chemistry and Physics

journal homepage: www.elsevier.com/locate/matchemphys

Grain boundary pinning of polycrystalline Al_2O_3 by Mo inclusions

Ching-Jang Lin, Wen-Cheng J. Wei*

Department of Materials Science and Engineering, National Taiwan University, 1 Roosevelt Rd. Sect. 4, Taipei 106, Taiwan, ROC

ARTICLE INFO

Article history:
Received 29 October 2007
Received in revised form 26 February 2008
Accepted 23 March 2008

Keywords:
Alumina
Molybdenum
Gradient
Structure
Nano-composite
Grain boundary pinning

ABSTRACT

Nano- to submicron-sized Mo particulates were deposited on porous Al_2O_3 disks in gradient concentration. The disks were laminated and sintered in inert atmosphere, revealing Mo inclusions in various contents and pining phenomena of matrix Al_2O_3 grains. Detail quantification of the microstructure of Mo and Al_2O_3 grains was conducted with special emphasis on the effects of the ultrafine Mo grains. The results show that the contents (5 vol% and 16 vol%) and the size of Mo inclusion are the critical quantities for the formation of intergranular/intragranular Mo inclusions. The microstructural development of the Al_2O_3 composites is greatly influenced by the states of the inclusions. A discussion on the topological and two other models of microstructural development is presented.

1. Introduction

Ceramic composites with nano-sized second-phase inclusion are reported [1,2] to have good mechanical properties and are more reliable with the help of microstructural improvements in several aspects, for instance, the reduction of inherent flaw size [2,3]. Second-phase inclusions (pores or particulates) that intersect the boundary act as a barrier to the boundary migration of matrix grains. *Zener* relation depicts the situation where the pores or second-phase inclusions in constant size are immobile [4–8]. As the grain boundary of matrix grains migrates toward their center of curvature with a driving force, the inclusions exert opposite restraining force (a drag force) on the boundaries. The grain boundary encountered the inclusions must stop while the acting forces reach an equilibrium condition. The drag force is exactly opposite to the driving force at grain size G_L of a well-developed matrix. The following *Zener* relation is obtained [6].

$$G_L = \frac{4r}{3V_f} \tag{1}$$

This simple relationship, but not an exact expression, shows that the limitation of grain growth decreases as the effective size (r) of the inclusions decreases and the volume fraction (V_f) increases.

A topological pinning model has been applied to Al_2O_3–SiC composite system containing monosized, spherical SiC inclusions, which are inert, immobile, and coarsening-resistant, showing the limiting grain size (G_L) [7,8] of the matrix as

$$G_L = K_t \frac{r}{(\phi_p V_f)^{1/3}} \tag{2}$$

where K_t is a proportionality constant, ϕ_p the fraction of particles at pinning positions, and V_f is the particle volume fraction. This is an expression of strong pinning relationship than that predicted by previous *Zener* pinning, which predicts the grain sizes to be much smaller for a given volume fraction [7,8].

Al_2O_3 and Mo are selected as a model system for this study. Mo being inert to Al_2O_3 at sintering temperature is the optimal choice for making metal/Al_2O_3 composites. Besides, due to the high electrical conductivity, high melting point, high Young's modulus, and low mismatch of thermal expansion of Mo to Al_2O_3, several Mo reinforced Al_2O_3 composites have been prepared and investigated in literatures [9–12]. Those have demonstrated significant improvements on the fracture strength and toughness of fine Mo/Al_2O_3 mixtures. However, the segregation and growth of nano-sized inclusions are still not well known yet, and need systematic investigation.

The deposition of Mo-species through a gaseous route has generating a gradient distribution of Mo-species in Al_2O_3 granules [13,14]. Similar approach is taken in this study to deposit the Mo into porous Al_2O_3 disk. Therefore, a model system, a porous Al_2O_3 disk infiltrating with Mo particulates, is adapted and used to prepare and sinter the layer structure, which allows us to investigate the possible influence of Mo inclusions at various fractions and sizes to the grain growth of polycrystalline Al_2O_3 matrix.

* Corresponding author. Tel.: +886 2 33661317; fax: +886 2 363 4562.
E-mail address: wjwei@ntu.edu.tw (W.-C.J. Wei).

0254-0584/$ – see front matter © 2008 Elsevier B.V. All rights reserved.
doi:10.1016/j.matchemphys.2008.03.029

2. Experimental

Porous Al_2O_3 disks were used as Mo-impregnated matrix, which were prepared and supplied by Leatec Fine Ceramics Co., Ltd., Taiwan, ROC. The disk-shape samples have the dimension of 0.5 mm (thickness) × 50 mm (diameter) and pre-sintered at 1100 °C to show 63% theoretical density (TD). Molybdenum hexacarbonyl ($Mo(CO)_6$, Alfa Chemicals Co., Newburyport, MA, USA) was used as the deposition source of Mo. The melting and boiling points of the $Mo(CO)_6$ powder are 150 °C and 156.4 °C (at 766 mm Hg), respectively.

The details of the metal-organic chemical vapor deposition (MOCVD) processes have been reported in our previous paper [13]. In order to deposit various amounts of Mo and to densify the layer composites, several processing conditions were selected. The deposition period of Mo-species varied from 0.5 h to 4.0 h (normally at 1.0 h) at 325 °C. The disks were stacked face-to-face and fixed with acrylic polymer (3 M, repositionable adhesive) before sintering. Then the stacks were hot-pressed under 4 MPa at the temperatures ≤1600 °C for 1.0 h in H_2 atmosphere. The hot-pressing furnace equipped with graphite heating elements which would react with H_2 at temperatures >1600 °C. Therefore, the furnace only operated at ≤1600 °C.

The microstructure and composition of the sintered bulks were analyzed by a TEM (100CXII, JEOL Co., Japan) and a SEM (XL30, Philips Co., Holland) equipped with an X-ray energy dispersive spectroscopy (EDS, DX-4, EDAX Co., USA). The elemental distribution of Al and Mo were also analyzed by an electron probe X-ray microanalyser (EPMA, JXA-8600, JEOL, Japan) which operated at 15 keV with an electron probe size of 1 μm and a current of 1×10^{-7} A.

Quantitative microstructural analysis selected the grains on the TEM and SEM micrographs. The grains were selected from the intercepts by the lines drawn parallel to the deposition surface of the disk samples. The statistical results, including average grain size ($\bar{d}$) of Mo or Al_2O_3 grains, were measured using the line-intercept method of the metallographic analysis reported in literature [15]. The Mo content was quantified from EDS spectra integrated from at least two line-scanning operations. The EDS analysis was calibrated by a set of standard samples containing the Mo contents up to 20 vol% [12].

3. Results and discussion

3.1. Concentration distribution of Mo

In order to systematically investigate the size distribution of Mo and the influence of Mo grains on Al_2O_3 matrix, a series of infiltrated Mo/Al_2O_3 disks were prepared and densified. Fig. 1 shows the SEM micrographs of the polished cross-section of one laminated Mo/Al_2O_3 composite. The densified composite shows the thickness of one disk of 360 μm (Fig. 1(a)). The features in Fig. 1(b) with brighter points due to a strong back scattering effect compared to Al element are the Mo inclusions. As the micrographs appear, the grain size of Mo decreases gradually from submicron to nano-size as the content of Mo decreases from the surface to the center of each disk. Besides, the EPMA results of Al and Mo elemental concentrations along the cross-section are shown in Fig. 1(c). The concentration of Mo gradually decreases from the surface to the depth of 20 μm, where no Mo inclusions are detected. The microstructure depicts a gradient change of Mo concentration and Mo grain size from the surface to the interior of the composite.

Fig. 2 shows the deposition content ($g\,cm^{-2}$) of Mo on the surface of the Al_2O_3 varied with the deposition time from 0.5 h to 4.0 h. The result exhibits the content of Mo on the surface of Al_2O_3 disk is a linear function of the deposition time. That depicts that the Mo content on the Al_2O_3 disk is controllable. The deposition flux at the deposition temperature 325 °C and at a constant gas pressure of 100 Torr was estimated from the slope of the fitting line in Fig. 2, being $5.63 \times 10^{-4}\,g\,cm^{-2}\,h^{-1}$ (i.e. $3.72 \times 10^{-9}\,mol\,cm^{-2}\,s^{-1}$).Our previous analysis [16] revealed that the surface deposition was controlled by a surface (pyrolysis) reaction of MoC_xO_y catalyzed by Al_2O_3. The diffusion of the gaseous Mo-species into the capillary of the porous matrices should belong to a Knudsen diffusion at 325–350 °C [13]. As the solid Mo particles were formed, no apparent inward diffusion of Mo species occurs at sintering stage to modify the distribution of Mo content. We assume the flux of gaseous molecules by a Knudsen diffusion at

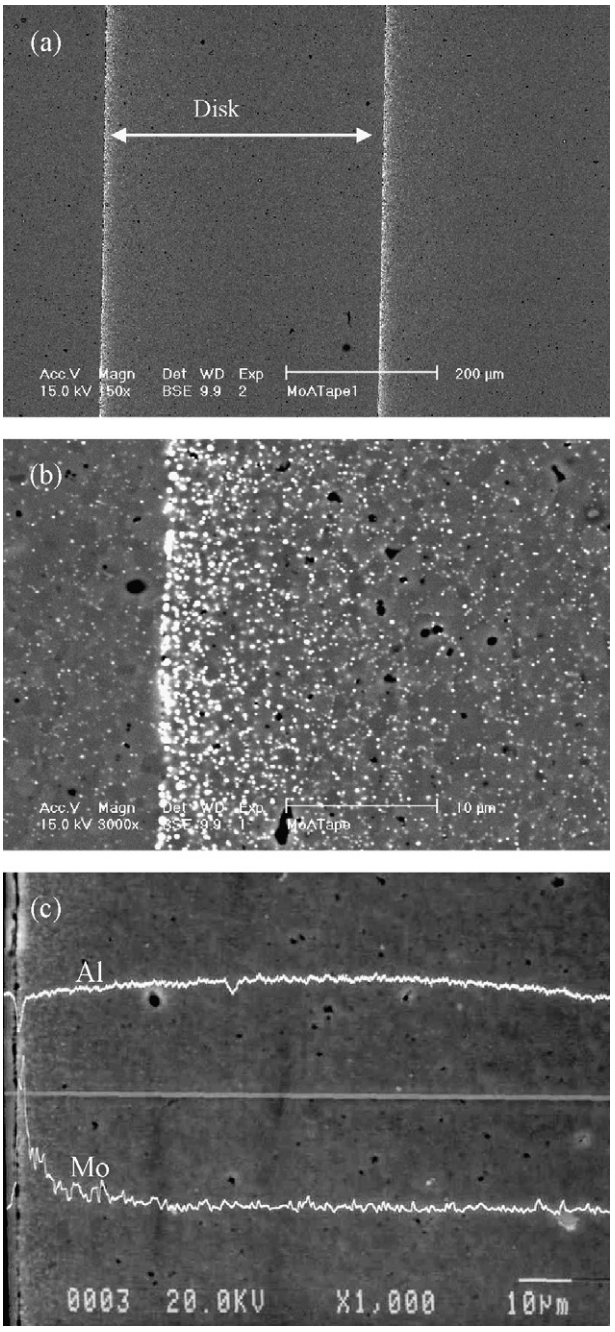

Fig. 1. (a) and (b) SEM micrographs, (c) EPMA Al and Mo elemental profiles of the cross-section of laminated Mo/Al_2O_3 structure. The specimens were MOCVD at 325 °C for 0.5 h, then stacking face-to-face and hot-pressed at 4 MPa and 1600 °C for 1.0 h in H_2 atmosphere. The thermally etched conditions were at 1400 °C for 20 min in H_2 atmosphere.

sintering temperature (1600 °C) should several orders higher than that ($1.5x10^{-3}$) shown at deposition temperatures (325-350 °C). Therefore, no gas species transport during the sintering of the composite.

3.2. Grain coarsening

The quantified results of the average grain size of Al_2O_3 are shown in Fig. 3. The grain size of Al_2O_3 increases from the surface (i.e., the volume fraction of Mo decreases). The results also show that the average grain size (G_m) of Mo has the similar trend as the

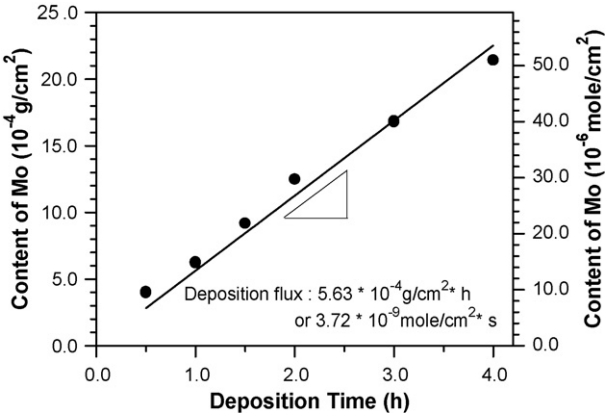

Fig. 2. Deposition content of Mo on the surface of Al_2O_3 varied with deposition time. The result was determined by metallographic method.

volume fraction of Mo (V_f). Meanwhile, the samples by MOCVD deposition for 2.0 h, 1.5 h, 1.0 h and 0.5 h all show the same trend, implying that the average grain size of Mo and Al_2O_3 is a function of the volume fraction of Mo.

The degree of retardation in the growth of Al_2O_3 grains depends on the grain size and on the volume fraction of Mo inclusions. According to *Zener* relation (Eq. (1)), the smaller the particle size and the more the volume fraction of Mo, the greater the degree of the grain-growth retardation [5,6]. The dragging force (F_G) of some large Mo inclusions is strong enough to pin the grain boundaries of Al_2O_3. In the mean time, the Mo inclusions are dragged by Al_2O_3 grain boundaries, and finally coalesce together. Only the nano-sized Mo inclusions are enclosed in the growing Al_2O_3 grains. In opposite conditions, the large Mo grains or a greater volume fraction of fine Mo grains tend to stay at Al_2O_3 grain boundaries, resulting in smaller Al_2O_3 grains throughout the entirely sintering process.

Fig. 4 shows the grain size of Al_2O_3 (G_a) as a function of the volume fraction of Mo (V_f). The diagram also reveals three inclined lines, corresponding to *Zener*, *Harmer*, and topological relations [7,8], whereas the slope of these lines are −1.0, −0.71, and −0.33,

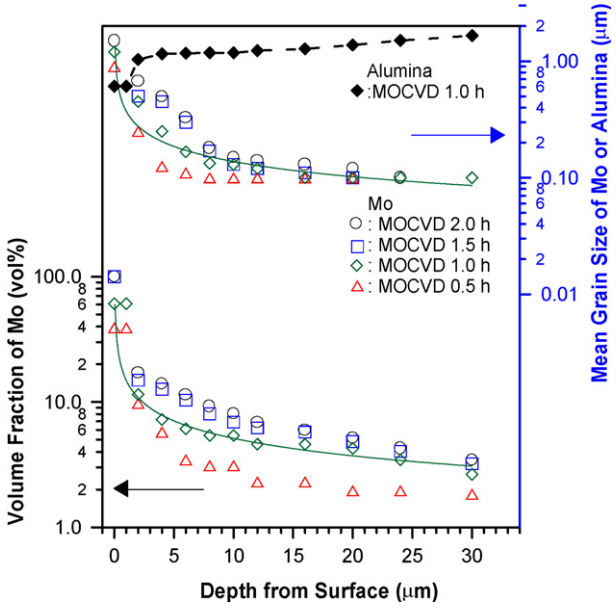

Fig. 3. Volume fraction (V_f) and mean grain size of Mo (G_m) grains on grain boundaries, and Al_2O_3 grain size varied with the depth from the surface of laminated disks.

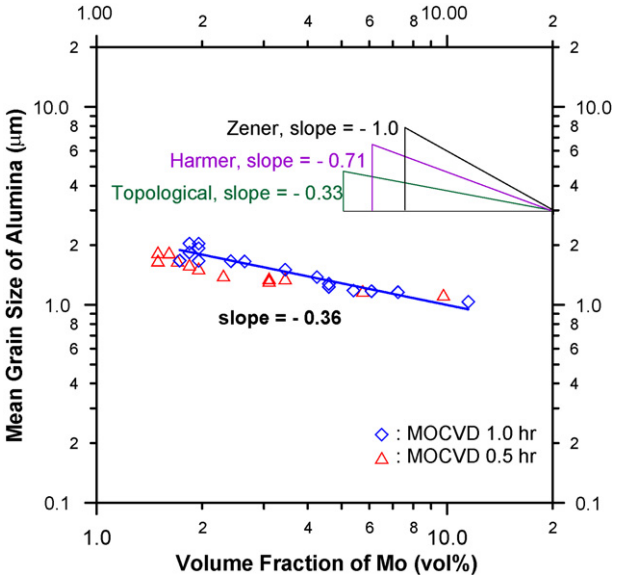

Fig. 4. Mean grain size of Al_2O_3 (G_a) versus volume fraction of Mo (V_f) on grain boundaries, and three predicted relations for Zener, Harmer [7,8], and topological models.

respectively. The best-fitting line of the experimental data shows a slope of −0.36 close to that of topological relation (Eq. (2)). The data obtained from the experiments hot-pressing at 1600 °C for 1.5 h might be not long enough to allow the grain sizes reaching fully development. That might result in slightly difference on the slope to the value (−0.33) predicted by the topological relation.

The relationship between the volume fraction of Mo (V_f) and the mean grain size (G_m) of Mo is presented in Fig. 5. The Mo grains are mainly categorized into two groups, either inter- or intragrains. The mean grain size of inter-granular Mo grains keeps nearly constant (i.e. 0.1 μm) as the V_f is smaller than the critical volume fraction, 5 vol%. A typical micrograph is shown in Fig. 6(a), in which the Mo grains on grain boundaries have distinct size preference. The G_m of intergranular Mo increases with an increasing of V_f as the V_f exceeds 5 vol%. In the following section, we tend to examine the dependence of Al_2O_3 grain size (G_a) on the effective volume fraction ($\phi_p V_f$) of Mo shown in the topological pinning model.

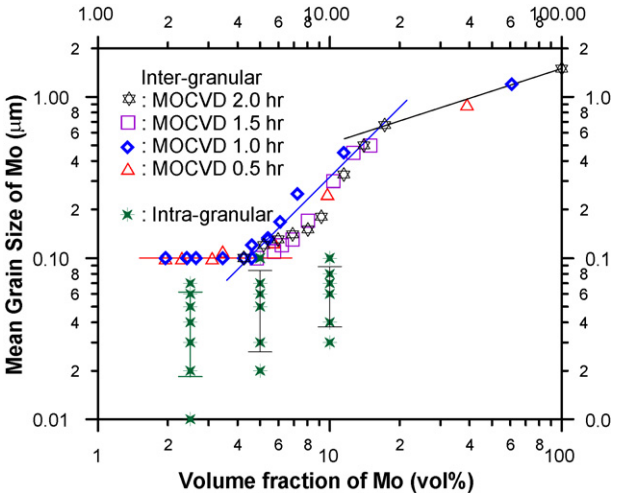

Fig. 5. Mean grain size of Mo (G_m) as a function of volume fraction (V_f) of the laminated disks with various deposition periods. The Mo grains are distinguished as either intergranular or intragranular.

As the content of Mo grains is less than 5 vol%, most of Mo grains in nano-sized (<100 nm) are enclosed in Al_2O_3 grains, as shown in Fig. 6(b). The nano-sized Mo grains are not able to pin the grain boundary movement of Al_2O_3 since the early stage of densification. Therefore, the G_m at grain boundaries equals to 0.1 μm in the Mo/Al_2O_3 case, as shown in Fig. 6. When the content of Mo phase is greater than 5 vol% and less than 16 vol%, the dragging force [6] from the intergranular Mo grains is

$$F_r = 2\pi\gamma r f(\theta) n_s \quad (3)$$

where γ is the surface energy, r the radius of the Mo grains, n_s the number of Mo grains on the grain boundary of Al_2O_3 per unit area, and $f(\theta)$ is a geometric fraction revealing the interactive area between boundary and inclusion. Basically, $f(\theta)$ shows the values between 0 and 0.5, which is the maximal interaction when the dragging force equals to the driving force (F_a) coming from the curvature ($G_a{}^{-1}$) of Al_2O_3 grains.

By the suggestions in literature [17], the relations appear as below.

$$F_a = \frac{\gamma}{G_a} \quad (4)$$

$$n_s = n_v r \quad (5)$$

and

$$V_f = n_v \left(\frac{4}{3}\right)\pi r^3 = n_s \left(\frac{4}{3}\right)\pi r^2 \quad (6)$$

where the n_v is the number of Mo grains per unit volume and r the grain size (i.e. G_m) of pining grain. In addition, the grain size of Al_2O_3 (G_a) is proportional to $V_f^{-0.36}$ (Fig. 4), and defined as

$$G_a = kV_f^{-0.36} \quad (7)$$

where k is a constant. If we assume the grain boundary with Mo inclusions is in equilibrium, then

$$F_a = F_r \quad (8)$$

Substitute Eqs. (4)–(8) into (3), we get

$$G_m = \left(\frac{3}{2}\right) k f(\theta) V_f^{0.64} \quad (9)$$

The size of the Mo grains to the volume percentage holds an exponent relationship of 0.64 as the volume of Mo is between 5 vol% and 16 vol%. The exponent value, 0.64, in Eq. (9) is fairly close to the inverse value of the slop (0.68) of the fitting line (16 vol% > V_f > 5 vol%) in Fig. 5.

It is also noted that the other turning point of Mo size/content dependence in Fig. 5 is 16 vol%. According to the percolation theory, 16 vol% can be considered as the threshold amount of second-phase connection in percolation state for a random packing in three dimensions. The coarsening of the Mo grains is thought that the grain growth is enhanced by the coalescence of neighbor Mo grains. However, large Mo grains retard the boundary movement of Al_2O_3 in greater force. It results that the Mo and Al_2O_3 grains are hardly growing when the V_f is greater than 16 vol%.

The maximum grain size of Mo only appear as the Mo-content is >16 vol%. The consequent microstructure of laminated composite appears that the amount of Mo is the major controlling factor to the final size of the inclusions either in nano-sized or submicron-sized.

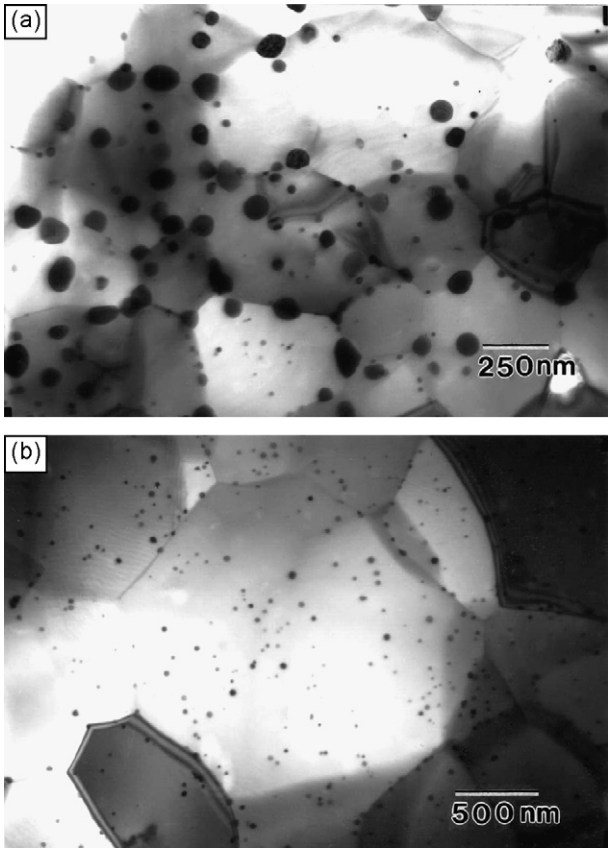

Fig. 6. TEM micrographs of the Mo/Al_2O_3 composites with vapor deposition period of (a) 2.0 h or (b) 1.0 h at 325 °C.

4. Conclusions

Layer Mo/Al_2O_3 composites with various Mo contents were prepared and investigated quantitatively. The nano-sized Mo grains coalesce to larger size as the Al_2O_3 matrix is densified. Large Mo grains (>0.1 μm) are trapped at Al_2O_3 boundaries when the composite is in the final stage of sintering processing. But, nearly all nano-sized (<100 nm) Mo grains are enclosed in Al_2O_3 grains. The coarsening of Mo and Al_2O_3 grains are closely relating to the content of the Mo in the composite.

As the content of Mo is less than 5 vol%, most of the Mo grains is in nanometric sizes, and the Mo forms fine inclusions in Al_2O_3 grains. The Al_2O_3 grains grow apparently due to minor Mo content. As the content of Mo (V_f) exceeds 5 vol%, the average particle size of Mo is larger than 100 nm. It is because of the coalescence of neighbor Mo grains is enhanced by the boundary movement of growing Al_2O_3 grains.

The Mo and Al_2O_3 grains are growing to nearly constant sizes when the V_f is more than 16 vol%. Large Mo grains retard the grain growth of matrix Al_2O_3. The average grain size of the Al_2O_3 is minimal as the content of Mo is reaching or more than 16 vol%. A two-phase Mo/Al_2O_3 layer composite with the microstructure of fine grain Al_2O_3 and Mo inclusions in controlled gradient distribution is demonstrated.

Acknowledgments

The authors would like to acknowledge the research funding given by National Science Council (NSC) in Taiwan under the contract NSC88-2216-E-002-028 and NSC96-2221-E-002-160-MY2. Helpful discussion and comments by Professor K.S. Huang at NTU and Dr. C.H. Hsueh at Oak Ridge National Laboratory are also appreciated.

References

[1] R. Roy, R.A. Roy, D.M. Roy, Alternative perspectives on quasi-crystallinity: non-uniformity and nanocomposites, Mater. Lett. 4 (1986) 323–328.
[2] K. Niihara, New design concept of structural ceramics–ceramic nanocomposites, J. Ceram. Soc. Jpn. 99 (10) (1991) 947–982.
[3] Y. Kinemuchi, T. Yanai, K. Ishizaki, In situ formation of Si_3N_4-nano SiC composite, Nanostruct. Mater. 9 (1996) 23–32.
[4] R.J. Brook, Pores and grain growth kinetics, J. Am. Ceram. Soc. 52 (6) (1969) 339–340.
[5] R.J. Brook, Pores-grain boundary interactions and grain growth, J. Am. Ceram. Soc. 52 (1) (1969) 56–57.
[6] Y.M. Chiang, D. Birnie III, W.D. Kingery, Physical Ceramics, John Wiley & Sons, New York, NY, USA, 1997, pp. 371–391.
[7] L.C. Stearns, M.P. Harmer, Particle-inhibited grain growth in Al_2O_3–SiC. I. Experimental results, J. Am. Ceram. Soc. 79 (12) (1996) 3013–3019.
[8] L.C. Stearns, M.P. Harmer, Particle-inhibited grain growth in Al_2O_3–SiC. II. Equilibrium and kinetic analyses, J. Am. Ceram. Soc. 79 (12) (1996) 3020–3028.
[9] M. Nawa, T. Sekino, K. Niihara, Improvement of fracture toughness of Al_2O_3/Mo nanocomposites, J. Mater. Sci. 29 (1994) 3185–3192.
[10] M. Nawa, K. Yamazaki, T. Sekino, K. Niihara, A new type of nanocomposite in TZP–Mo system, Mater. Lett. 20 (1994) 299–304.
[11] W.C.J. Wei, S.C. Wang, F.H. Cheng, Microstructural development of Al_2O_3-compoistes with fine Mo particulates. I. Microstructural development, Nanostruct. Mater. 10 (6) (1998) 965–981.
[12] S.C. Wang, W.C.J. Wei, Microstructural development of Al_2O_3-compoistes with fine Mo particulates. II. Densification and mechanical properties, Nanostruct. Mater. 10 (6) (1998) 983–1000.
[13] C.J. Lin, C.C. Yang, W.C.J. Wei, Processing and microstructure of nano-Mo/Al_2O_3 composites from MOCVD and fluidized bed, Nanostruct. Mater. 11 (8) (1999) 1361–1377.
[14] C.J. Lin, W.C.J. Wei, T. Iwai, C.W. Hong, P. Greil, DEM simulation and processing of nano-Mo/Al_2O_3 granules in fluidized bed, Proc. Natl. Sci. Council ROC (A) 24 (5) (2000) 394–404.
[15] J.C. Wurst, J.A. Nelson, Lineal intercept technique for measuring grain size in two-phase polycrystalline ceramics, J. Am. Ceram. Soc. 55 (2) (1972) 109.
[16] W.J. Wei, M.H. Lo, Processing and properties of (Mo,Cr) oxycarbides from MOCVD, Appl. Organomet. Chem. 12 (1998) 201–220.
[17] D.S. McLachlan, M. Blaszkiewicz, R.E. Newnham, Electrical resistivity of composites, J. Am. Ceram. Soc. 73 (8) (1990) 2187–2203.